Analysis of the Effect of Geometry Generated Turbulence on HCCI Combustion by Multi-Zone Modeling

S. M. Aceves, D. L. Flowers, J. Martinez-Frias, F. Espinosa-Loza, M. Christensen, B. Johansson, R. P. Hessel

December 15, 2004

Disclaimer

This document was prepared as an account of work sponsored by an agency of the United States Government. Neither the United States Government nor the University of California nor any of their employees, makes any warranty, express or implied, or assumes any legal liability or responsibility for the accuracy, completeness, or usefulness of any information, apparatus, product, or process disclosed, or represents that its use would not infringe privately owned rights. Reference herein to any specific commercial product, process, or service by trade name, trademark, manufacturer, or otherwise, does not necessarily constitute or imply its endorsement, recommendation, or favoring by the United States Government or the University of California. The views and opinions of authors expressed herein do not necessarily state or reflect those of the United States Government or the University of California, and shall not be used for advertising or product endorsement purposes.

Analysis of the Effect of Geometry Generated Turbulence on HCCI Combustion by Multi-Zone Modeling

Salvador M. Aceves, Daniel L. Flowers,
Joel Martinez-Frias and Francisco Espinosa-Loza
Lawrence Livermore National Laboratory

Magnus Christensen and Bengt Johansson
Lund Institute of Technology

Randy P. Hessel
University of Wisconsin-Madison

Abstract

This paper illustrates the applicability of a sequential fluid mechanics, multi-zone chemical kinetics model to analyze HCCI experimental data for two combustion chamber geometries with different levels of turbulence: a low turbulence disc geometry (flat top piston), and a high turbulence square geometry (piston with a square bowl). The model uses a fluid mechanics code to determine temperature histories in the engine as a function of crank angle. These temperature histories are then fed into a chemical kinetic solver, which determines combustion characteristics for a relatively small number of zones (40). The model makes the assumption that there is no direct linking between turbulence and combustion.

The results show that the multi-zone model yields good results for both the disc and the square geometries. The model makes good predictions of pressure traces and heat release rates. The experimental results indicate that the high turbulence square geometry has longer burn duration than the low turbulence disc geometry. This difference can be explained by the sequential multi-zone model, which indicates that the cylinder with the square bowl has a thicker boundary layer that results in a broader temperature distribution. This broader temperature distribution tends to lengthen the combustion, as cold mass within the cylinder takes longer to reach ignition temperature when compressed by the expansion of the first burned gases. The multi-zone model, which makes the basic assumption that HCCI combustion is controlled by chemical kinetics, is therefore capable of explaining the experimental results obtained for different levels of turbulence, without considering a direct interaction between turbulence and combustion. A direct connection between turbulence and HCCI combustion may still exists, but it seems to play a relatively minor role in determining burn duration at the conditions analyzed in this paper.

Introduction

The nature of HCCI combustion has been the topic of multiple publications over the last 25 years. The initial publications that identified HCCI as a distinct combustion phenomenon [1,2] described HCCI as an autoignition process that initiates simultaneously at multiple sites and then spreads quickly through the remaining of the combustion chamber. These publications also conducted spectroscopy studies that show that the different radicals appear sequentially, in contrast with SI combustion where all radicals appear simultaneously at a given point.

Najt and Foster [3] analyzed the information presented by [1, 2] and concluded that these results can be explained by assuming that HCCI combustion is dominated by chemical kinetics, with pressure, temperature and species concentration determining the ignition timing. This opens the possibility of conducting chemical kinetics-based analysis of HCCI combustion, which was applied by Najt and Foster to determine the sensitivity of ignition timing to multiple operating parameters.

The model by Najt and Foster was adopted and extended by some of the authors of this paper [4]. HCCI combustion is described as dominated by chemical kinetics. Turbulence is likely to play a role on HCCI ignition, as turbulent temperature fluctuations may be large enough to initiate local combustion in small volumes [1, 2, 5, 6]. However, turbulence plays a minor role on combustion once ignition occurs. After ignition, combustion propagates from the initial ignition points as a pressure wave. Unburned fuel and air are compressed and heated as the hot burned gases expand after combustion. Compression heating of the unburned gases is typically enough to burn all of the fuel, except for fuel in the crevices and boundary layer, which is too cold to ignite [7, 8]. According to this description, there is no flame propagation in HCCI combustion, since a flame is typically defined as a thin combustion front that spreads through diffusion of energy and radicals from the burned zone to the unburned zone [9]. This conclusion is supported by experimental results [5] that indicate that the speed of propagation of the combustion front in HCCI is much higher than any deflagration speed found in SI engines. Turbulence does play an indirect role on HCCI combustion, by altering the temperature distribution and the boundary layer thickness within the cylinder. Turbulence therefore indirectly determines the speed of combustion, as different volumes in the cylinder ignite in succession from the hottest to the coldest due to compression heating.

The HCCI description detailed in the previous paragraph appears to have gained acceptability among researchers. It is now generally accepted that a chemical kinetics-based combustion model is applicable for HCCI combustion, as long as the air and fuel are well mixed in the cylinder and no significant mass stratification exists [10]. If mass stratification exists, turbulence plays a more direct role on combustion [11, 12], as discontinuities (such as flames) may exist that are convected and deformed by turbulence. The chemical kinetic model of HCCI combustion may still be applicable to partially stratified engines (commonly known as premixed charge compression ignition, PCCI engines [13]), as long as the degree of stratification is relatively small.

The fact that turbulence plays a relatively minor role on HCCI combustion greatly simplifies the analysis of HCCI engines. Accurate analysis of HCCI can be achieved with a full integration between a fluid mechanics code and a chemical kinetics code. In a fully integrated approach, the fluid mechanics code calculates temperature distribution and mixing, while the chemical kinetics code calculates composition and heat release in every cell. The fact that HCCI combustion is relatively insensitive to turbulence makes it possible to use a relatively coarse grid (millimeter-size cells), as the cell size is determined by the need to appropriately resolve the temperature distribution in the cylinder. In contrast, SI and diesel engines need to be analyzed with much finer grids (possibly micron-size cells), as it is necessary to resolve the interaction between the very thin flame fronts and the turbulence field. However, even the coarser grids required for HCCI combustion (with ~50,000 cells for a 2-dimensional mesh or ~500,000 cells for a 3-dimensional mesh) are too big for today's computers. Full integration of a fluid mechanics code with a chemical kinetics code may be the method of choice for HCCI analysis in the future, as fast, highly parallelized computers may be able to tackle the very high computational intensity of this problem. However, for now, fully integrated calculations are limited to small chemical kinetic mechanisms (~100 species) and coarse grids (~1000 cells) [13, 14].

An alternative to full integration of a fluid mechanics code and a chemical kinetics code for HCCI analysis is to use a multi-zone model. In a multi-zone HCCI analysis, cells that have similar pressure, temperature and composition histories are grouped into a relatively small number of zones (10-100). The chemical kinetics solver is then applied to this small number of zones, instead of the large number of cells typically used in fluid mechanics codes. Considering that conducting chemical kinetics calculations is much more computationally expensive than conducting fluid mechanics calculations (Figure 1), it can be concluded that the multi-zone model can offer great advantage in computational time with respect to a full integration of a chemical kinetics code and a fluid mechanics code.

Previous work by the authors [7, 8] has focused on developing and validating multi-zone models for HCCI combustion. The results have shown considerable success in predicting combustion and emissions over multiple geometries, fuels, and operating conditions.

In this paper, the multi-zone model is applied to analyze the results of a recent experiment [15] in which an HCCI engine was run with two different piston geometries to study the effect of turbulence on HCCI combustion. The two geometries are a low turbulence flat-top piston and a high turbulence piston with a square bowl. Recently, these experiments have been analyzed [14] by using a fully integrated fluid mechanics-chemical kinetics code. This fully integrated model predicted combustion with good accuracy for the high turbulence and the low turbulence geometries. A relatively coarse grid with a reduced chemical kinetic mechanism was used, due to the high computational cost of the method. The multi-zone model makes it possible to analyze the results from the turbulence experiments with a high resolution grid and a detailed chemical kinetic model. On the down side, the multi-zone model implementation used for this work does not consider the effect of mixing after ignition, which plays a very minor role on

combustion, but has been shown to have an effect on HC and CO emissions [16]. The purpose of this paper is to test whether the multi-zone model can capture the effect of variable degrees of turbulence on HCCI combustion, with the purpose of contributing to a deeper understanding of the nature of HCCI combustion.

The Experiment

The two cylinder geometries used in this study are produced with interchangeable piston crowns, which make it possible to use the same piston body [17, 18]. Figure 2 shows a sketch and Figure 3 a photograph of the piston crown with the square bowl. In the square bowl the swirling flow is believed to break up into smaller eddies in the corners. This eddy break-up generates high amounts of small scale turbulence. The squish distance with the square bowl combustion chamber is only 1 mm, giving a strong squish motion. Figures 4 and 5 show the flat piston crown, i.e. with a disc combustion chamber. For the disc combustion chamber the swirling flow is expected to be more or less undisturbed during the compression and expansion stroke. The squish distance is 12 mm with the disc combustion chamber. The combustion chambers will be referred as Square and Disc in the remaining of the paper. Table 1 lists the main dimensions for the two crowns.

The experiment [15] included runs for naturally aspirated and supercharged conditions. In this paper we only analyze the supercharged cases, which used 2 bar absolute intake pressure iso-octane fuel, 0.4 equivalence ratio and 11.2:1 compression ratio. Since the in-cylinder turbulence and mean velocities are functions of crank angle, the combustion phasing was varied from early timing with steep pressure rise to very late timing with noticeable cycle to cycle variations. Combustion phasing was varied by changing the intake temperature with an electric heater. The engine speed was set to 1200 rpm at all conditions.

The single cylinder test engine is based on an in-line 6 cylinder Volvo™ TD100 truck engine. The major engine specifications are shown in Table 2. The port fuel injector was placed approximately 300 millimeters upstream of the inlet valve. The inlet air temperature was adjusted with an electric heater mounted upstream of the fuel injector.

The cylinder pressure was measured with a Kistler® 7061B pressure transducer via a Kistler™ 5011 charge amplifier. For each test condition, the pressure was recorded for 100 cycles, every 0.2 degrees crank angle. The pressure data was analyzed using a single zone heat release model [19].

The experiments also included in-cylinder flow measurements to determine turbulence levels. The velocity measurements were performed with a two component DANTEC™ fiber-flow system illuminated by an Ar-ion laser. The measuring volume length was about 0.7 mm and the diameter about 0.05 mm. More on the LDV system specifications can be found in [17].

Optical access to the combustion chamber was through a quartz window with a 10 mm diameter placed in the location where the diesel fuel injector is normally mounted. The LDV measurement volume was located 5 mm below the cylinder head and had a 20 degree angle from the vertical axis. Figure 6 shows the measurement position and the obtained velocity components. The optical layout accurately measures the tangential (y-component) velocity, but the tilting from the vertical axis causes the radial (x-component) velocity to be influenced by the axial velocity.

The seeding used was a polystyrene-latex dispersion in water. The mean polystyrene particle size was 0.28 μm and the mean droplet size from the liquid atomizers was 3 – 4 μm. The dry weight of the dispersion was less than 1 %, which means that the resulting dry particle size was below 1 μm. The obtained data rate was approximately 5 – 7 bursts per crank angle.

The Model

Figure 7 illustrates the overall sequence of calculations required for the multi-zone method. The procedure is started by making a fluid mechanics code run (KIVA3V, [20]) considering motored (no ignition) conditions. The resulting geometric temperature distribution, shown in Figure 7(a), is then converted into a temperature mass distribution. The temperature mass distribution gives the fraction of the total mass in the cylinder that has a certain temperature. Figure 7(b) shows a typical temperature mass distribution at TDC and a cumulative mass distribution, which indicates the fraction of the mass that is colder than a specified temperature T. The mass within the cylinder is then assigned to temperature zones. The number of zones is selected, as well as a mass distribution within the zones. For this work, the mass was distributed among 40 zones. Previous research has shown that 40 zones are necessary to properly resolve the small regions of the cylinder where HC and CO are typically produced [21]. The computational expense of using 40 zones has been considerably reduced by the development of a segregated solver [22]. A 40-zone run with a detailed iso-octane mechanism takes 1 day on a single processor of a 2 GHz computer running Linux.

The temperature-weighted mass distributions are calculated from KIVA3V for multiple crank angles during the compression stroke. These temperature distributions are used for calculating zone temperature histories. Figure 7(c) shows a temperature history for 10 of the 40 zones. The temperature histories are the geometry-specific information that is passed from KIVA3V to the chemical kinetics code (HCT; Hydrodynamics, Chemistry and Transport [23]) to yield results that satisfactorily consider the effects of both fluid mechanics and chemical kinetics. HCT is run in multi-zone mode starting at intake valve closing and continuing until the end of the expansion stroke. The zones in HCT follow the temperature histories obtained from KIVA3V during the compression stroke, until the point of ignition (defined as the crank angle at which the cumulative energy release reaches 5% of the total available chemical energy). After ignition, the KIVA3V

temperature histories are abandoned and pressure and zone temperatures are determined from basic thermodynamic equations [22] and the Woschni heat transfer correlation [24]. HCT calculates all combustion parameters, including pressure, burn duration, heat release, combustion efficiency, exhaust emissions, radical concentration (Figure 7(d)) and all the details about the chemical kinetics during HCCI combustion. The model as applied here does not consider the effect of mixing between zones after ignition. Before ignition, mixing between zones is handled through the use of the KIVA3V temperature histories.

Three grids were generated for the disc geometry. These are a baseline grid (54,000 elements), a 0.5X resolution grid (14,000 elements), and a 2X resolution grid (210,000 elements). The grids were tested against experimental data for both motored cases and firing cases, and little difference was observed between the three grids. Due to the favorable agreement, the baseline grid was used for all the results presented. Figure 8 shows the axisymmetric baseline grid. For the square bowl, only a single grid was made with 0.5X resolution and 410,000 elements. This is a 3-dimensional 90 sector mesh (Figure 9). No other grids were generated for the square geometry due to the extremely long computational time that it takes to run this very large grid (about 3 weeks in a single processor of a 2 GHz Linux computer). It is expected that this grid can deliver accurate results, since the resolution is the same as the 0.5X grid used for the disc geometry, which yielded good results. The chemical kinetics code (HCT) uses a detailed chemical kinetics model for iso-octane that includes 859 species and 3606 chemical reactions [25].

Pressure traces are matched by adjusting the temperature at intake valve closing (IVC) to obtain the appropriate ignition timing. Pressure at IVC may also be slightly adjusted to obtain a good match for the peak cylinder pressure. The same initial pressure and temperature were used for all the zones. Composition at IVC was determined by taking into account the effect of residual gases. No other parameters are adjusted in the model, and all the default parameters are used in KIVA3V for wall heat transfer, turbulence, etc. The chemical kinetic mechanism is used in its original form with no modifications.

Results

Figure 10 shows a comparison between experimental and numerical results for turbulence intensity as a function of crank angle, for the square and the disc geometries. The turbulence intensity is measured and calculated at the point indicated in Figure 6, 5 mm off the cylinder axis. Experimental results are shown by solid lines and numerical results by dotted lines. The figure shows that KIVA3V accurately predicts turbulence intensity for the disc geometry. However, the prediction for the square geometry is not as good, with KIVA3V predicting earlier phasing of the peak turbulence intensity and considerably overpredicting the turbulence intensity. The difference in turbulence intensity can be qualitatively explained by considering that KIVA3V takes into account the three components of turbulence, while the experiments only measured the x and y components. The z (axial) component was not measured. Visualization of the KIVA3V results shows that for the disc geometry the z component of turbulence is likely a small contributor to the overall turbulence intensity, as the swirling flow remains fairly

undisturbed during the late part of the compression stroke. On the other hand, it is considered that for the square geometry the z component of turbulence is likely to be a large contributor to the turbulence intensity, due to the turbulence induced by bowl squish flows. These considerations are consistent with the good results obtained for the disc engine and the relatively poor agreement obtained for the square engine. While this may be responsible for the differences between the analysis and the experimental results, this effect cannot be quantified, as KIVA3V calculates only turbulence intensity and not the individual components of turbulence. Other effects that may exist in the experiment but are not considered in KIVA3V, such as tumble flows, may also affect the results.

Figures 11, 12 and 13 show a comparison between experimental and numerical results for the disc geometry. Figure 11 shows experimental pressure traces (solid lines) and numerical pressure traces (dotted lines). The figure shows good agreement in all cases. Heat release rates are also well predicted (Figure 12). Burn duration is quite well predicted, although the maximum rate of heat release is underpredicted by 10-20% in all cases. Figure 13 shows the ratio between numerical and experimental results for carbon monoxide emissions, hydrocarbon emissions and combustion efficiency. A ratio of 1 in Figure 13 indicates a perfect agreement. Figure 13 shows that combustion efficiency is well predicted and HC emissions are reasonably well predicted. For the high load HCCI conditions being analyzed here, HC emissions originate mainly at the crevices, which are too cold to react [8]. Carbon monoxide emissions are underestimated by a factor of 4-10, because the current implementation of the multi-zone model does not consider diffusion between zones after the point of ignition. Unburned HC from the crevices can potentially diffuse into the hot core gases in the cylinder, reacting partially to form CO emissions. Recent work [16] has demonstrated that including diffusion between zones in the model considerably improves prediction of HC and CO emissions in this high load operating range.

Figures 14, 15 and 16 show a similar set of results for the square geometry as has been shown in Figures 11-13 for the disc geometry. Figure 14 shows a comparison between experimental and numerical pressure traces for the square geometry. The figure shows good agreement between the experimental and the numerical results, although the agreement is not as good as in Figure 11 for the disc geometry. Figure 15 shows a comparison between experimental and numerical heat release rates for the square geometry. The results compare well. Burn duration is well predicted, but peak heat release is once again underestimated by ~20%. Figure 16 shows the ratio between numerical and experimental values for HC, CO and combustion efficiency for the square geometry. The results are very similar to those of Figure 13. Combustion efficiency is well predicted, HC emissions are reasonably well predicted, and CO is underpredicted by a factor of 3-10.

Figures 17-19 show a comparison between experimental and numerical results for CO, HC and combustion efficiency for both the disc and the square geometries. This information is similar to the results presented in Figures 13 and 16, except that Figures 17-19 show absolute values instead of ratios, and information is now presented as a function of the crank angle for peak heat release. Figure 17 shows that CO emissions are

consistently underpredicted by the multi-zone model, by as much as a factor of 10 in some cases. These results are consistent with previous multi-zone results [4, 22]. As previously explained, CO predictions are low because the multi-zone model does not consider the effect of mixing between zones. At the high load HCCI conditions considered in this paper, unburned HC from the crevices can potentially diffuse into the hot core gases in the cylinder, reacting partially to form CO emissions. Only at very low loads can the multi-zone model make good predictions of CO emissions, because at low loads CO is not generated by mixing. Instead, at low loads, when the combustion temperature drops below 1500 K, CO is produced in the bulk gases [26].

The experimental and numerical results for hydrocarbon emissions are shown in Figure 18. The figure shows reasonably good agreement, especially for the late combustion cases. HC emissions at the high load HCCI conditions considered here originate mainly in the crevices. HC predictions are therefore sensitive to wall temperature and crevice volume, which determine the mass of fuel in the crevices.

Figure 19 shows a comparison between experimental and numerical results for combustion efficiency. Combustion efficiency is well predicted in all cases; especially at the late combustion cases where HC emissions are best predicted (Figure 18). For the early combustion cases, the model slightly overpredicts combustion efficiency, as both HC and CO are underpredicted when combustion is advanced.

Figure 20 shows a comparison between numerical and experimental burn duration for the square and the disc geometries. Burn duration in the figure is defined as the crank angle interval between the two points where heat release is 10% of the peak heat release. As it may be expected by looking at the heat release curves (Figures 12 and 15), the numerical results give a good approximation to the experimental results, tracking the experimental results over the whole range of data and consistently overpredicting the experimental burn duration by only a fraction of a crank angle degree. The numerical results are also consistent with the experimental data in predicting a longer burn for the square geometry than for the disc geometry.

The longer burn obtained for the higher turbulence square geometry can be explained by considering the mass distribution in temperature shown in Figure 21. This figure shows the distribution of mass (i.e. what fraction of the total mass exists at any given temperature) at 6 BTDC, for both the square and disc geometries, for two pairs of conditions that have the peak heat release at nearly identical angles. This information is similar to the mass distribution shown in Figure 7(b), except that a linear scale is used in Figure 21 instead of a logarithmic scale. The first pair corresponds to the cases with Tin=443 K for the disc and Tin=431 K for the square geometry. Both of these cases have the peak heat release at ~3 degrees after TDC. The second pair is Tin=433 K for the disc and Tin=419 K for the square geometry. For this second pair of conditions, peak heat release occurs at ~8 ATDC. The figure shows that, in both cases, the temperature distribution is considerably narrower for the disc geometry than for the square geometry. This can be explained by the higher turbulence level in the square geometry (Figure 10), which tends to produce a thicker thermal boundary layer, which results in a broader

temperature distribution. The peak temperature is nearly the same in the cases that ignite at the same time.

The results presented in Figure 21 combined with the hypothesis that HCCI combustion is controlled by chemical kinetics explain the longer burn duration experimentally observed for the square bowl (Figure 20). The two pairs of conditions analyzed in Figure 21 have nearly the same maximum temperature, which explains the fact that they have similar ignition timing. After ignition, combustion spreads across the chamber as the colder mass in the cylinder heats up and sequentially ignites as it is compressed by the expansion of the first burned gas. From this description, it is easy to see that a broader temperature distribution produces longer burn duration, as more cold mass exists that requires further compression heating before ignition occurs. The assumption that HCCI combustion is controlled by chemical kinetics is therefore capable of explaining the experimental results obtained for different levels of turbulence, without the need to consider a direct interaction between turbulence and combustion. A direct connection between turbulence and HCCI combustion may still exist, but it seems to play a relatively minor role in determining burn duration at the conditions analyzed in this paper.

Discussion

The key assumption in simulation of HCCI is that the combustion process is controlled solely by chemical kinetics. In other words, turbulent mixing does not affect the chemical reactions and heat release process during the main chemical heat release process. The justification for this assumption is that the combustion in HCCI engines is a bulk autoignition process, i.e. ignition occurs with near simultaneity at many points throughout the combustion chamber. Thus, the chemical reactions that yield the main heat release occur so rapidly that the turbulent mixing does not have time to influence combustion.

The basis for the assumption that turbulence does not influence the heat release process comes from the fundamental nature of HCCI combustion. Spectroscopic investigation has shown that HCCI is a non-propagating, bulk, spontaneous autoignition process [2], while flame propagation processes such as spark-ignited combustion have been widely seen to occur with a flame front. The chemistry that occurs in this autoignition processes such as knock and HCCI is fundamentally the same as what occurs locally in a flame front - the key difference is in how the mixture is brought to temperatures that result in spontaneous ignition. The propagation of the flame front occurs as radicals and heat from the flame front region diffuse to initiate combustion in the neighboring unreacted mixture. It is important to notice that the neighboring mixture is typically not ready to react until the front diffuses into it. The chemistry and turbulent interactions are often characterized by non-dimensional parameters such as the Damköhler number, a ratio of turbulent time scales to chemical timescales. Large Damköhler (>>1) number means that chemistry is very fast compared to turbulent mixing, and thus turbulent mixing is the rate-limiting process. Thus for premixed flame propagation the mixture in the flame front

is in the fast-chemistry high Damköhler number regime, while the unburned mixture ahead of the flame is at a slow chemistry low Damköhler number regime. Thus, in flame propagation the Damköhler number regimes can be considered to be spatially distributed.

In an HCCI engine cycle the mixture also experiences low and high Damköhler regimes, but these are instead temporally distributed. Prior to ignition, chemistry is slow compared with mixing, so the trace species formed (e.g. H_2O_2) are well distributed throughout the mixture, i.e. the low Damköhler number regimes. Once the mixture reaches sufficient temperature, the chemistry accelerates rapidly, starting the rapid breakdown of the H_2O_2 into two OH radicals and the subsequent chain branching steps. In HCCI the entire mixture is brought to ignition temperature essentially at once by the compression process. Because the species created during the pre-ignition, distributed reaction, part of the cycle are well distributed throughout the mixture, the bulk mixture will be at near autoignition conditions when autoignition begins locally in the charge (likely at the highest temperature region in the combustion chamber gasses). Heat release from the first ignited mixture compresses the neighboring mixture as heat is released and local temperature and pressure is elevated. For HCCI combustion this compression must be sufficient to subsequently bring the rest of the combustion chamber to temperatures where autoignition will occur. The HCCI ignition process as described relies on the local chemistry occurring more rapidly than turbulent mixing rates. A good estimate local chemistry timescale in an HCCI autoigntion would be the time for local conversion of CO to CO_2, which for HCCI conditions will be on the order 1-10 microseconds. A local turbulent timescale can be taken from the integral length and timescale (approximately 10 milliseconds for most engines), which is very slow compared with the chemistry timescale [27]. A better estimate of local turbulent effects would be to use a timescale based on eddies on the order of the Taylor microscale, the scale usually associated with the mixing in thin flame fronts [27]. Even looking at the Taylor microscale, which is typically one to two orders of magnitude smaller than the integral length scale, results in mixing timescales of order 100 microseconds to 1 millisecond, which still shows that the local turbulent mixing is significantly slower than the local chemistry timescale.

Conclusions

This paper illustrates the applicability of a sequential fluid mechanics, multi-zone chemical kinetics model to analyze HCCI experimental data for two combustion chamber geometries with different levels of turbulence: a low turbulence disc geometry (flat top piston), and a high turbulence square geometry (piston with a square bowl). The model uses a fluid mechanics code to determine temperature histories in the engine as a function of crank angle. These temperature histories are then fed into a chemical kinetic solver, which determines combustion characteristics for a relatively small number of zones (40). The model makes the assumption that there is no direct linking between turbulence and combustion.

The results show that the multi-zone model yields good results for both the disc and the square geometries. The model makes good predictions of pressure traces and heat release rates. The experimental results indicate that the high turbulence square geometry has longer burn duration than the low turbulence disc geometry. This difference can be explained by the sequential multi-zone model, which indicates that the cylinder with the square bowl has a thicker boundary layer that results in a broader temperature distribution. This broader temperature distribution tends to lengthen the combustion, as cold mass within the cylinder takes longer to reach ignition temperature when compressed by the first burned gases. The multi-zone model, which is based on the assumption that HCCI combustion is controlled by chemical kinetics, is therefore capable of explaining the experimental results obtained for different levels of turbulence, without the need to consider a direct interaction between turbulence and combustion. A direct connection between turbulence and HCCI combustion may still exist, but it seems to play a relatively minor role in determining burn duration at the conditions analyzed in this paper.

References

1. Onishi, S., Jo, S. H., Shoda, K., Jo, P. D., and Kato, S., "Active Thermo-Atmosphere Combustion (ATAC) - A New Combustion Process for Internal Combustion Engines," SAE paper 790501, 1979.

2. Noguchi, M., Tanaka, Y., Tanaka, T., and Takeuchi, Y., "A Study on Gasoline Engine Combustion by Observation of Intermediate Reactive Products During Combustion," SAE paper 790840, 1979.

3. Najt, P. M. and Foster, D. E., "Compression-Ignited Homogeneous Charge Combustion," SAE paper 830264, 1983.

4. Aceves, S. M., Flowers, D.L., Westbrook, C.K., Smith, J. R., Pitz, W.J., Dibble, R., Christensen, M. and Johansson, B., "A Multi-Zone Model for Prediction of HCCI Combustion and Emissions," SAE Paper 2000-01-0327, 2000.

5. Hultqvist, A., Christensen, M., Johansson, B., Richter, M., Nygren, J., Hult, J., Alden, M., "The HCCI Combustion Process in a Single Cycle-High-Speed Fuel Tracer LIF and Chemiluminescence Imaging, SAE Paper 2002-01-0424, 2004.

6. Chen, J.H., Hawkes, E.R., Hewson, J.C., Sankaran, R., Im, H.G., Mason, S.D., "Ignition Front Propagation in a Constant Volume with Temperature Inhomogeneities," Proceedings of the Combustion Institute, Volume 30, 2004.

7. Aceves, S.M., Flowers, D.L., Espinosa-Loza, F., Martinez-Frias, J., Dibble, R.W., Christensen, M., Johansson, B., Hessel, R.P., "Piston-Liner Crevice Geometry Effect on HCCI Combustion by Multi-Zone Analysis," SAE Paper 2002-01-2869, 2002.

8. Aceves, S.M., Flowers, D.L., Espinosa-Loza, F., Martinez-Frias, J., Dec, J.E., Sjöberg, M., Dibble, R.W., and Hessel, R.P., "Spatial Analysis of Emissions Sources for HCCI Combustion at Low Loads Using a Multi-Zone Model," SAE Paper 2004-01-1910, 2004.

9. Turns, S.R., "An Introduction to Combustion, Concepts and Applications," Chapter 8, McGraw-Hill, New York, NY, 2000.

10. Christensen, M., Johansson, B., Amneus, P., and Mauss, F., "Supercharged Homogeneous Charge Compression Ignition," SAE Paper 980787, 1998.

11. Zhang, Y.Z., Kung, E.H., and Haworth, D.C., "A PDF Method for Multidimensional Modeling of HCCI Engine Combustion: Effects of Turbulence/Chemistry Interactions on Ignition Timing and Emissions," Proceedings of the International Multidimensional Engine Modeling User's Group Meeting, Detroit, MI, 2004.

12. Benkenida, A., and Angelberger, C., "Toward a Three-Dimensional CFD Model for HCCI Combustion in Diesel Engines," Combustion Science and Technology, Vol. 176, pp. 667-683, 2004.

13. Aceves, S.M., Flowers, D.L., Espinosa-Loza, F., Babajimopoulos, A., and Assanis, D., "Analysis of Premixed Charge Compression Ignition Combustion with a Sequential Fluid Mechanics-Multizone Chemical Kinetics Model," Submitted to the SAE Congress, 2005.

14. Kong, S.C., Reitz, R.D., Christensen, M., Johansson, B., "Modeling the Effects of Geometry-Generated Turbulence on HCCI Engine Combustion," SAE Paper 2003-01-1088, 2003.

15. Christensen, M., Hultqvist, A., Johansson, B., "The Effect of Combustion Chamber Geometry on HCCI Operation," SAE Paper 2002-01-0425.

16. Flowers, D. L., Aceves, S. M., Martinez-Frias, J., Hessel, R.P., and Dibble, R. W., "Effects of Mixing on Hydrocarbon and Carbon Monoxide Emissions, Predictions for Isooctane HCCI Engine Combustion Using a Multi-Zone Detailed Kinetics Solver," SAE Paper 2003-01-1821, 2003.

17. B. Johansson, K. Olsson: "Combustion Chambers for Natural Gas SI Engines Part I: Fluid Flow and Combustion", SAE950469

18. B. Johansson, K. Olsson: "Combustion Chambers for Natural Gas SI Engines Part II: Combustion and Emissions", SAE950517

19. B. Johansson: "On Cycle to Cycle Variations in Spark Ignition Engines", Ph.D. Thesis, ISRN LUTMDN/TMVK-1010-SE, Dept. of Heat & Power Engineering, Lund Institute of Technology, Sweden, 1995

20. Amsden, A.A., "KIVA-3: A KIVA Program with Block-Structured Mesh for Complex Geometries," Los Alamos National Laboratory Report LA-12503-MS, 1993.

21. Flowers, D. L., Aceves, S. M., Martinez-Frias, J., and Dibble, R. W., Prediction of Carbon Monoxide and Hydrocarbon Emissions in Iso-Octane HCCI Engine Combustion Using Multi-Zone Simulations," *Proc. Combust. Inst.*, Vol. 29, 2002.

22. Aceves, S.M., Martinez-Frias, J., Flowers, D.L., Smith, Dibble, R.W., Wright, J.F., and Hessel, R.P., "A Decoupled Model of Detailed Fluid Mechanics Followed by Detailed Chemical Kinetics for Prediction of Iso-Octane HCCI Combustion," SAE Paper 2001-01-3612, 2001.

23. Lund, C. M., "HCT - A General Computer Program for Calculating Time-Dependent Phenomena Involving One-Dimensional Hydrodynamics, Transport, and Detailed Chemical Kinetics," Lawrence Livermore National Laboratory report UCRL-52504, 1978.

24. Woschni, G., "Universally Applicable Equation for the Instantaneous Heat Transfer Coefficient in the Internal Combustion Engine," SAE Paper 670931, 1967.

25. Curran, H. J., Gaffuri, P., Pitz, W. J., and Westbrook, C. K., "A Comprehensive Modeling Study of Iso-Octane Oxidation," Combustion and Flame, Vol. 129, pp. 253-280, 2002.

26. Sjoberg 1500 K paper

27. Heywood, J. B., Internal Combustion Engine Fundamentals, McGraw-Hill, Inc., New York, NY, 1988.

Table 1. Piston Crown Specifications.

	Square	Disc
Squish Distance	1 mm	12 mm
Topland height	32 mm	21 mm
Cylinder wall area at TDC	323 cm^2	278 cm^2

Table 2. Engine specifications and operating conditions.

Displaced Volume	1600 cm^3
Bore	120.65 mm
Stroke	140 mm
Connecting Rod Length	260 mm
Number of Valves	2
Inlet Valve Diameter	50 mm
Exhaust Valve Diameter	46 mm
Exhaust Valve Open	39 BBDC (at 1 mm lift)
Exhaust Valve Close	10 BTDC (at 1 mm lift)
Inlet Valve Open	5 ATDC (at 1 mm lift)
Inlet Valve Close	13 ABDC (at 1 mm lift)
Valve Lift Exhaust	13.4 mm
Valve Lift Inlet	11.9 mm
Compression Ratio	11.2:1
Coolant Temperature	88 C
Oil Temperature	90 C
Engine Speed	1200 rpm
Fuel	Iso-octane
Equivalence Ratio	0.4
Intake pressure	2 bar absolute
IMEP	6.5-7.3 bar
Exhaust Pressure	2.3 bar
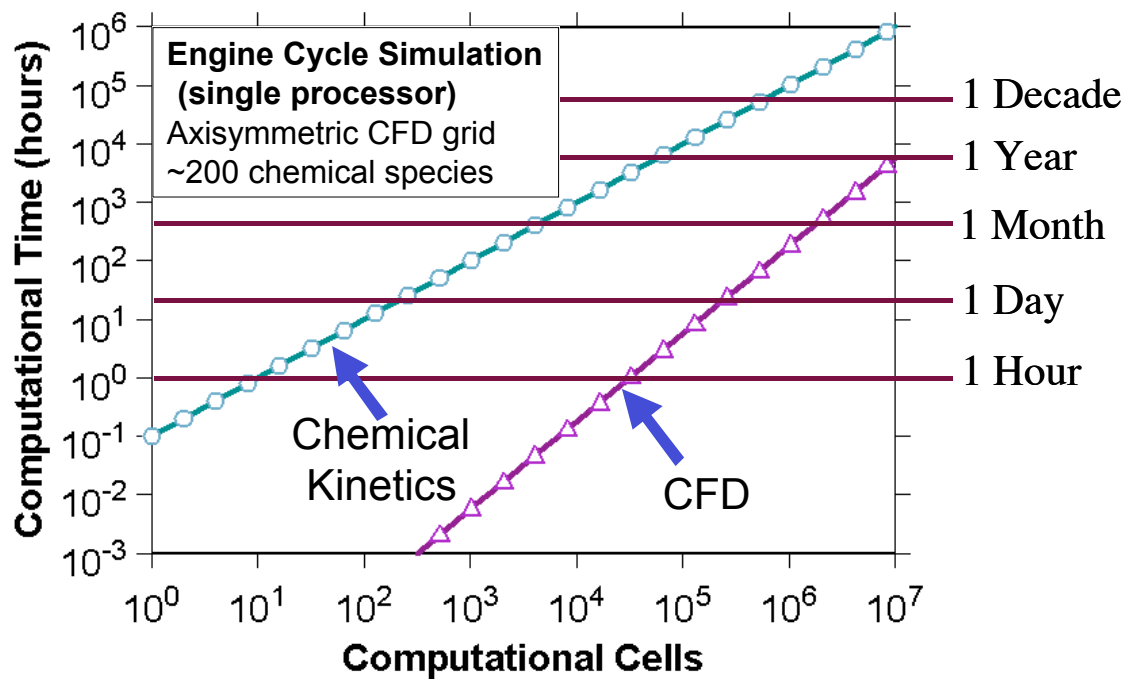
Figure 1. Computational time in a single processor of a 2 GHz LINUX computer as a function of the number of computational cells for a computational fluid mechanics (CFD) calculation and a chemical kinetics calculation.
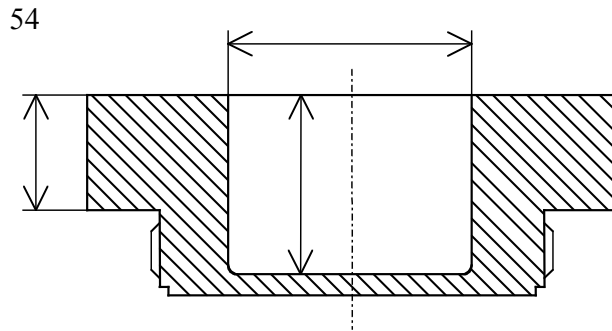
Figure 2. Sketch of the piston crown with square bowl.

Figure 3. Piston crown with square bowl combustion chamber.
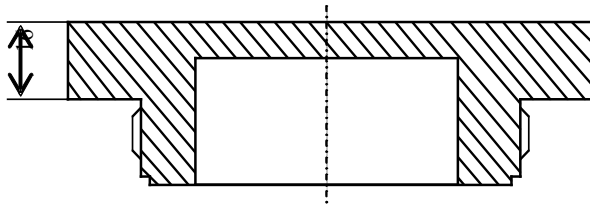
Figure 4. Sketch of the flat piston crown.

Figure 5. Flat piston crown used in the disc geometry.
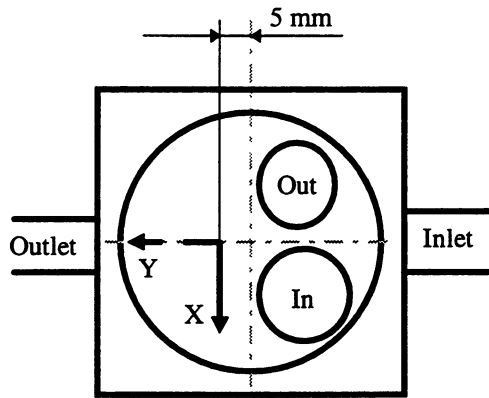
Figure 6. Picture showing the LDV measurement position for determining turbulence (seen from above) and the velocity components. The swirling flow in the engine is counterclockwise.
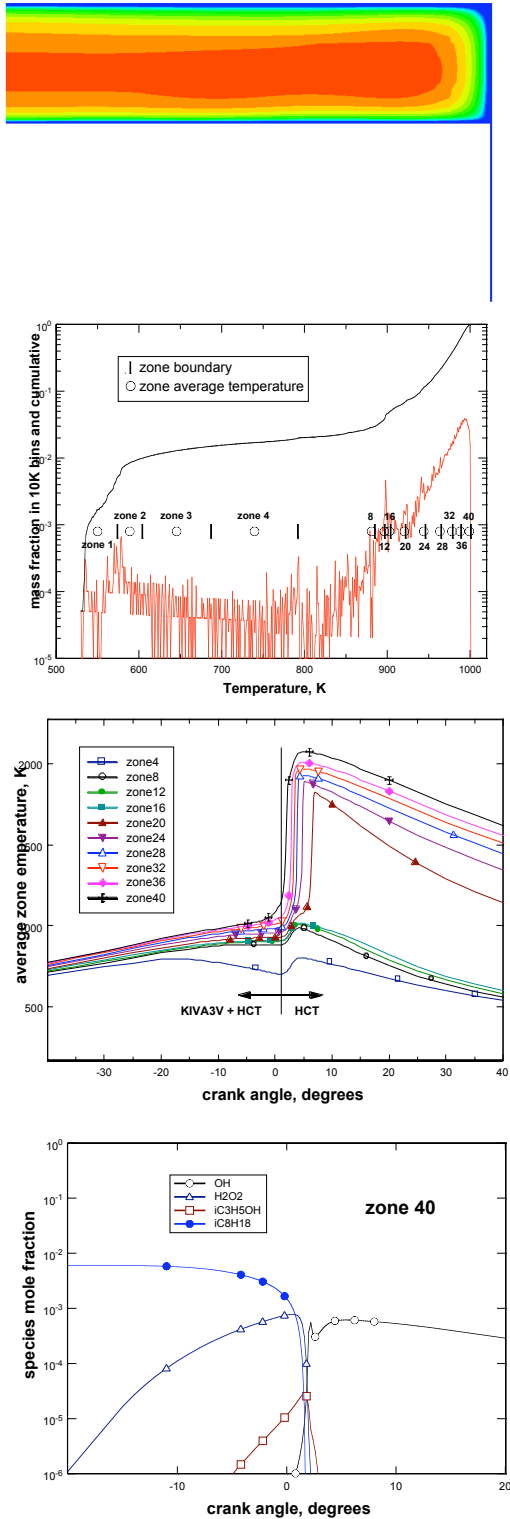
Figure 7. The main steps in the sequential multi-zone analysis of HCCI combustion. (a) Calculation of temperatures inside the cylinder from KIVA3V. (b) Calculation of mass distribution as a function of temperature. (c) Calculation of temperature histories for the zones. (d) Detailed chemical kinetics HCT run with temperature histories determined from KIVA3V.
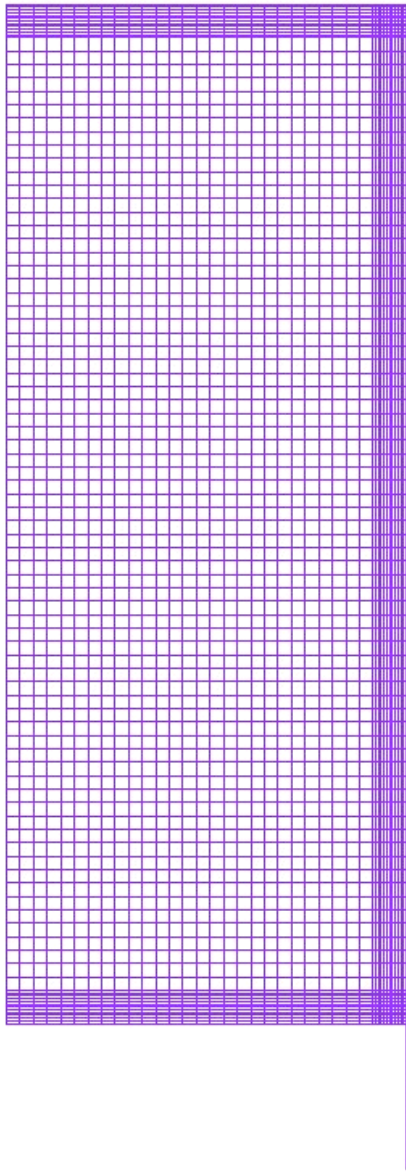
Figure 8. Baseline grid for disc engine, with 54,000 elements.
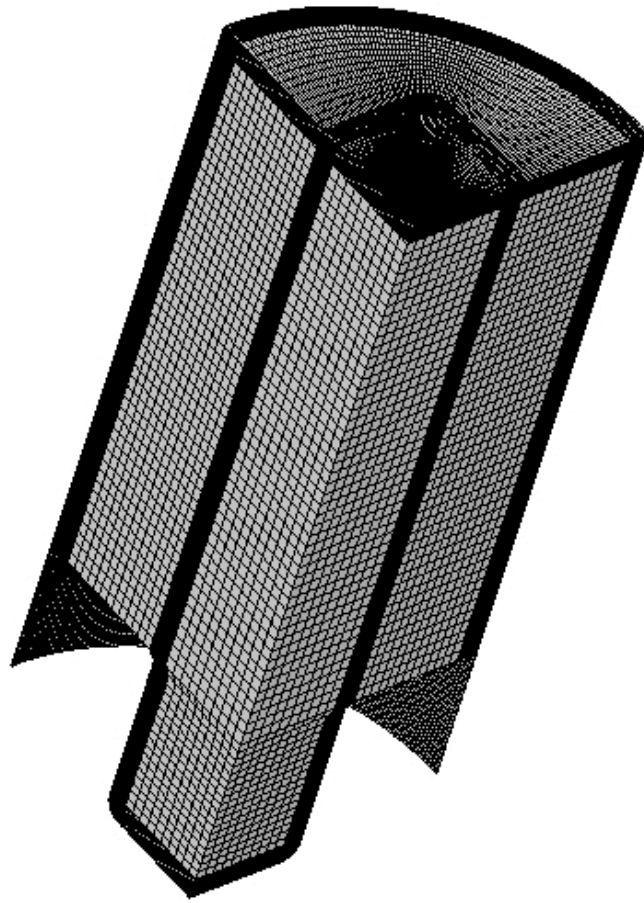
Figure 9. Three-dimensional 90 sector mesh for the square geometry, with 0.5X resolution and 410,000 elements.
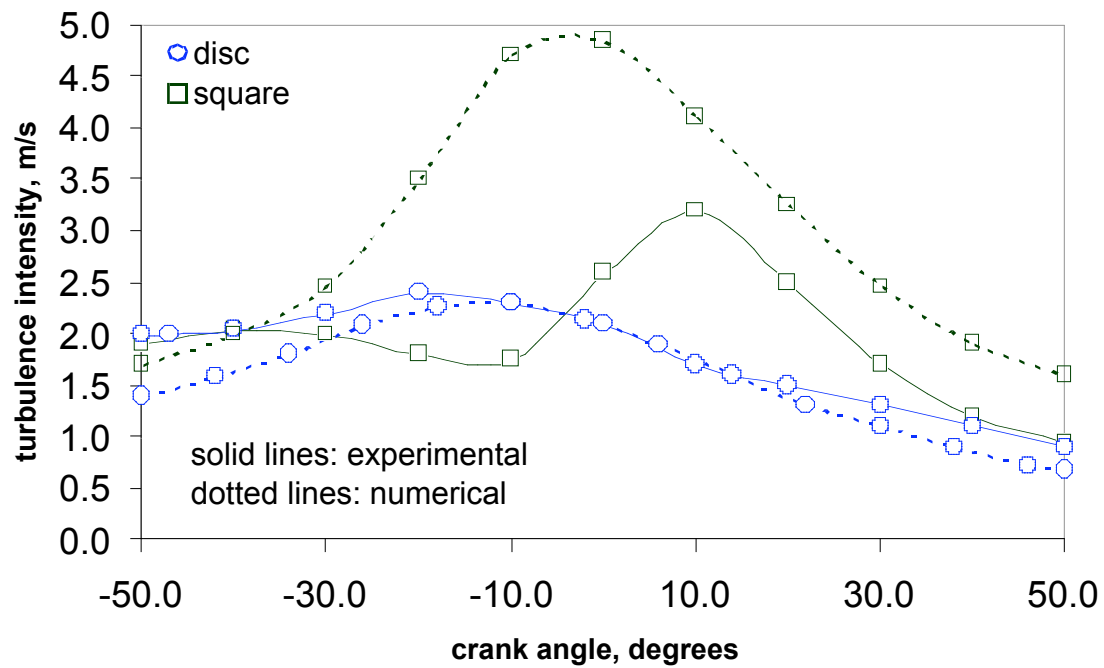
Figure 10. Comparison between experimental and numerical results for turbulence intensity as a function of crank angle, for the square and the disc geometries. The turbulence intensity is measured and calculated at the point indicated in Figure 6, 5 mm off the cylinder axis. Experimental results are shown by solid lines and numerical results by dotted lines.
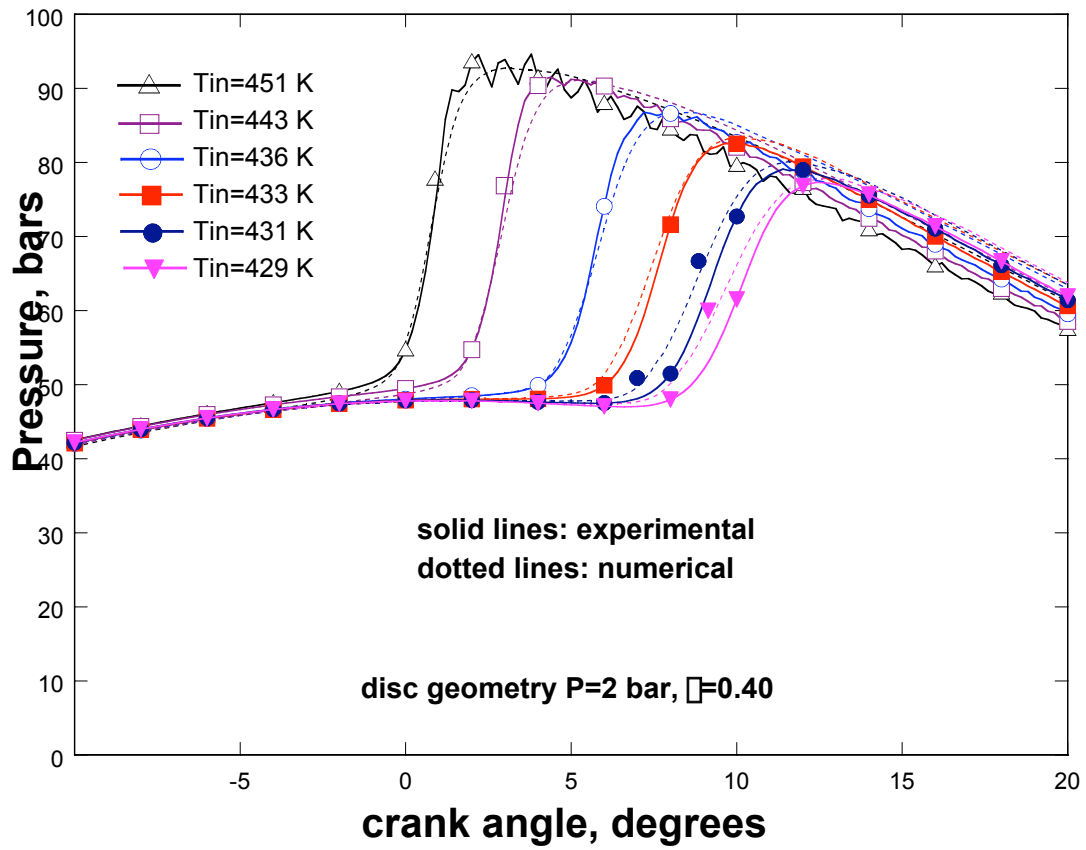
Figure 11. Comparison between experimental and numerical pressure traces for the disc geometry. The figure shows experimental pressure traces with solid lines and numerical pressure traces with dotted lines.
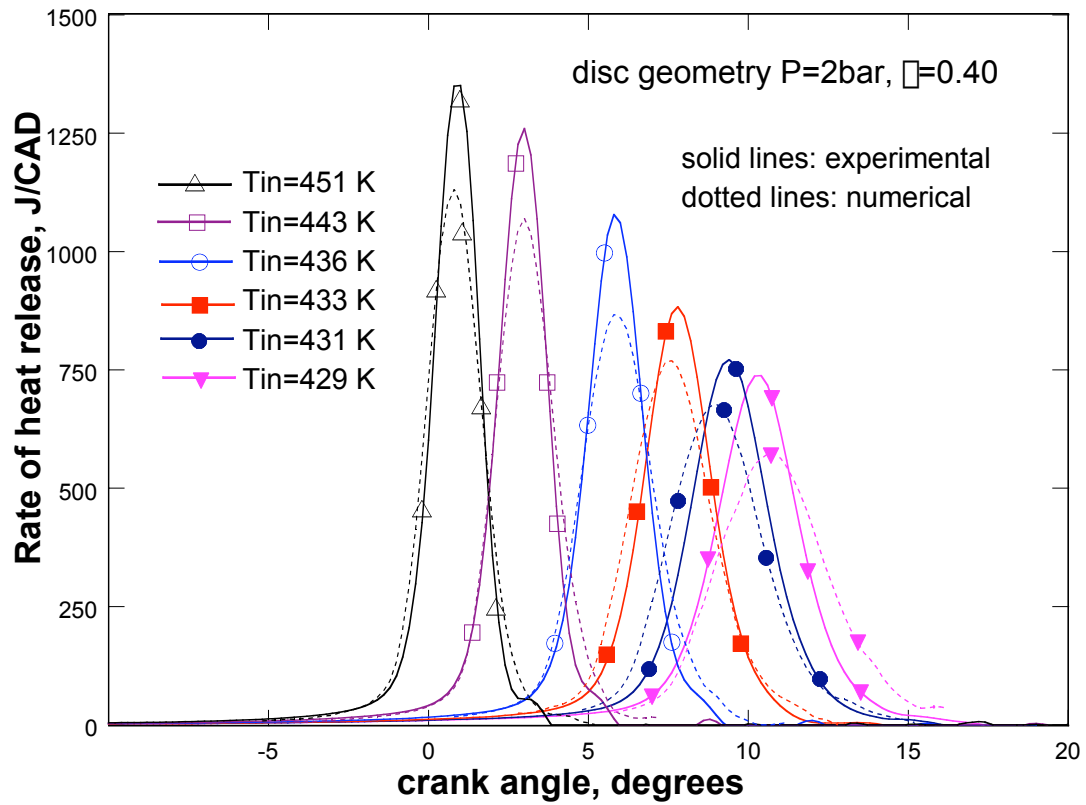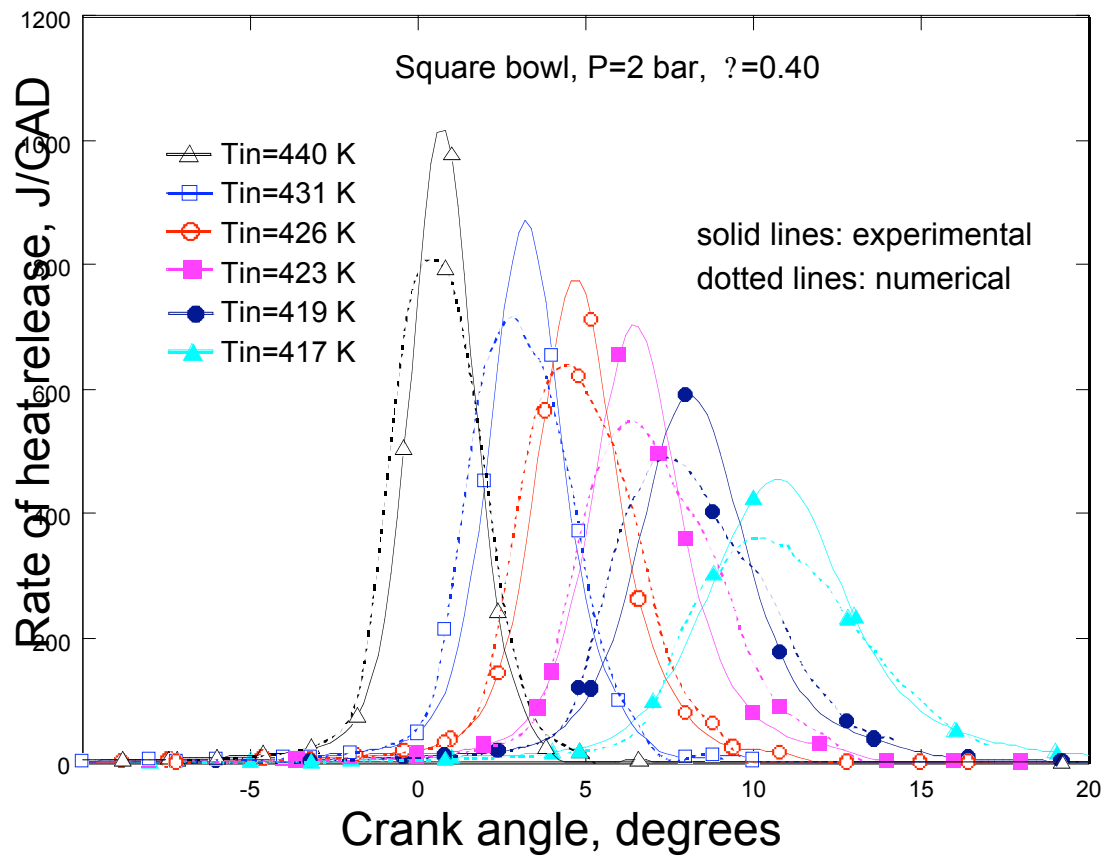
Figure 12. Comparison between experimental and numerical heat release rates for the disc geometry. The figure shows experimental heat release rates with solid lines and numerical heat release rates with dotted lines.
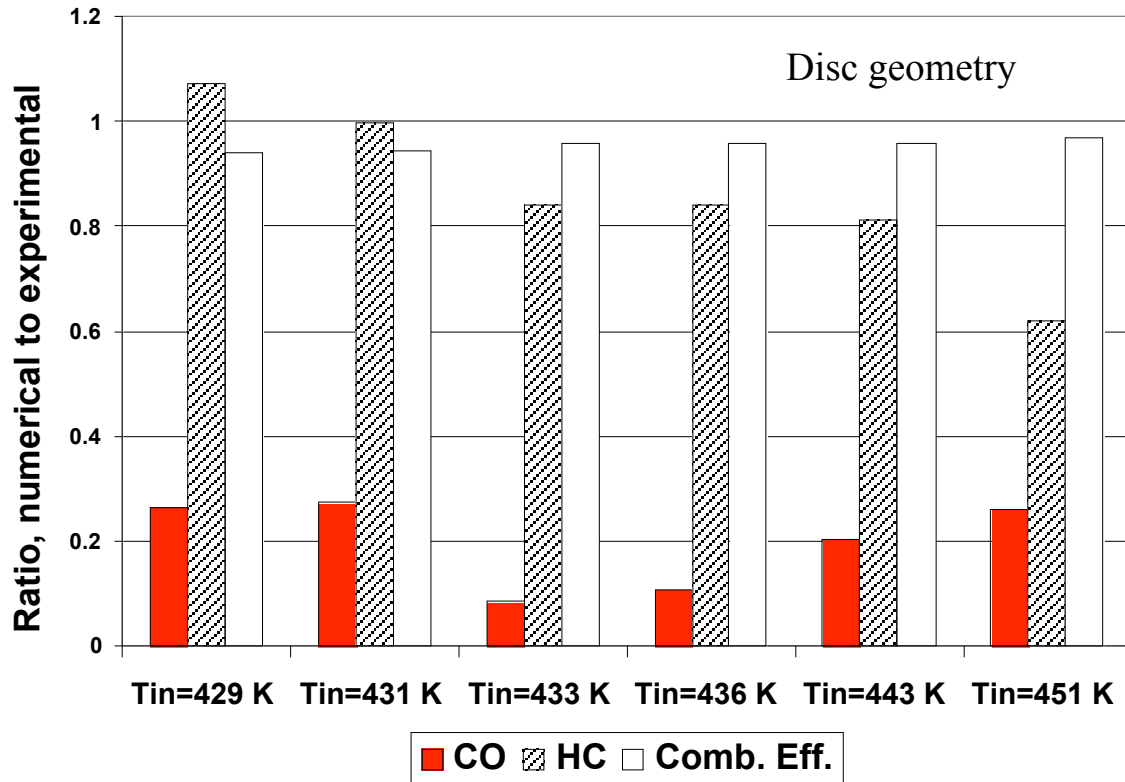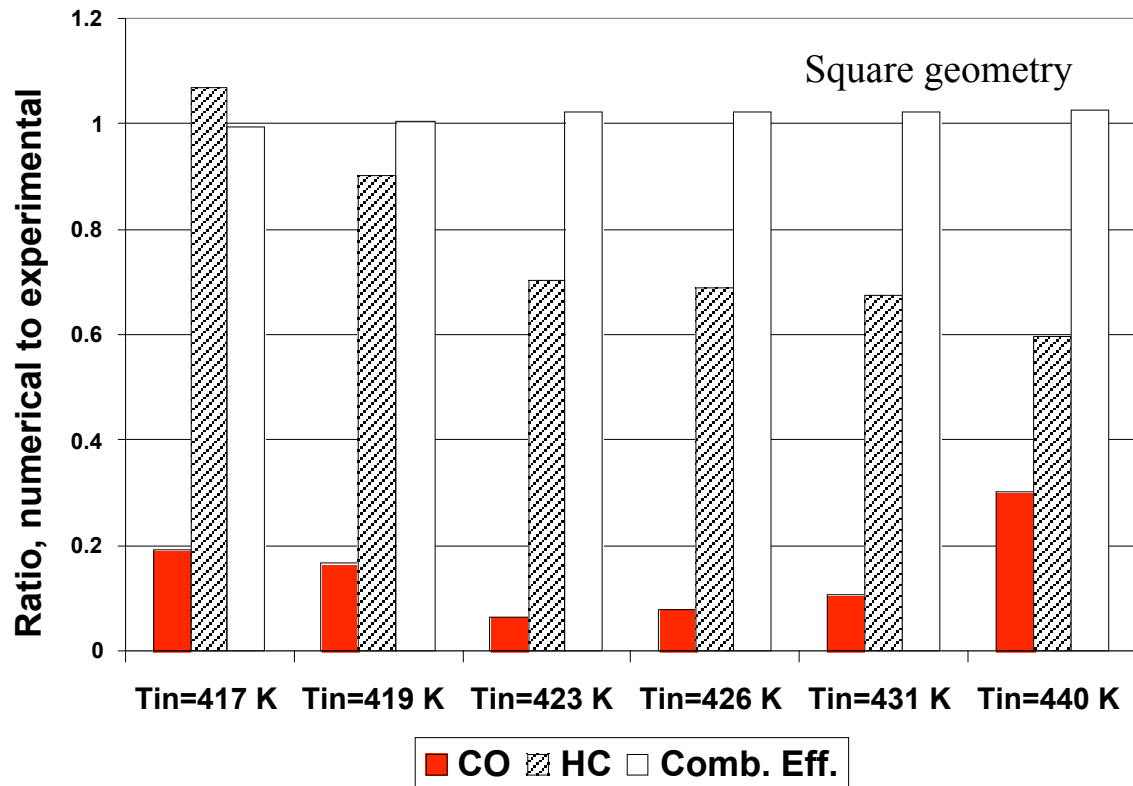
Figure 13. Ratio between numerical and experimental results for carbon monoxide emissions, hydrocarbon emissions and combustion efficiency, for the disc geometry. A ratio of 1 in the figure indicates perfect agreement between experimental and numerical results.
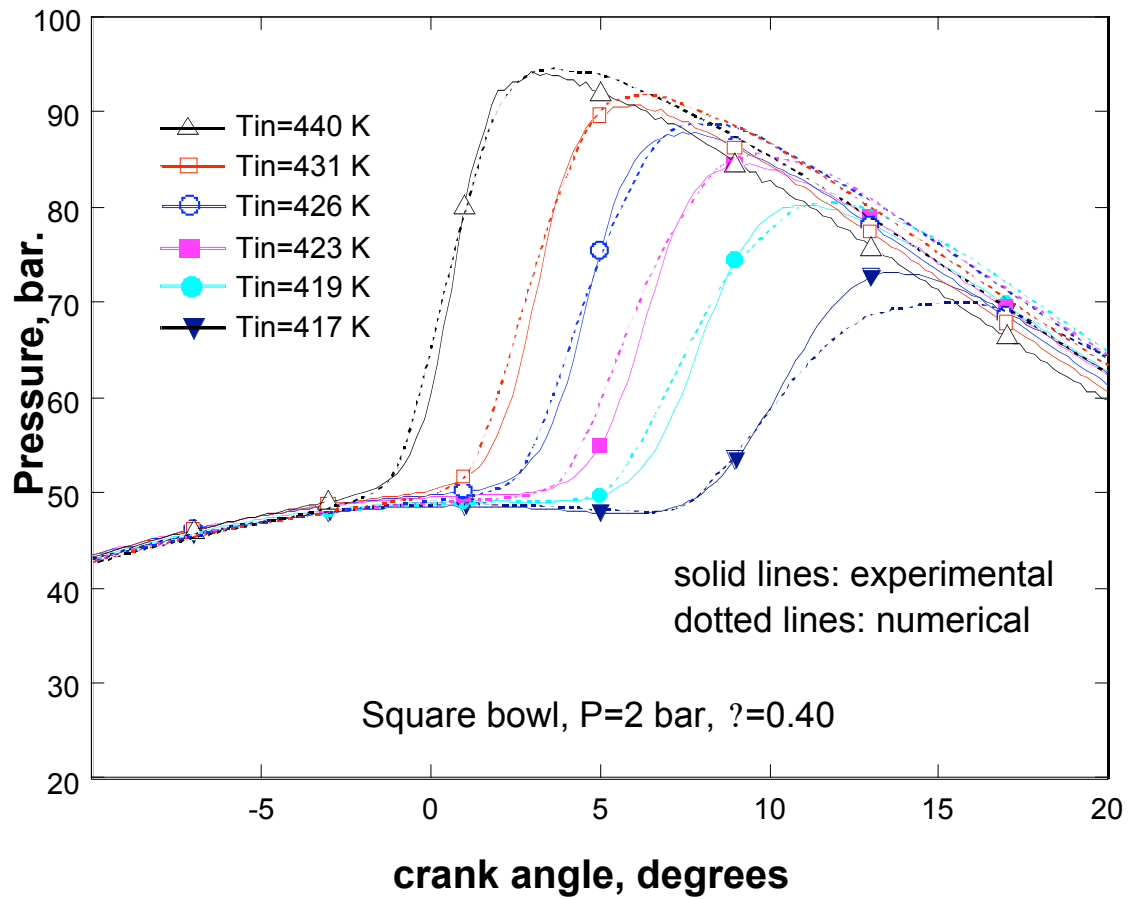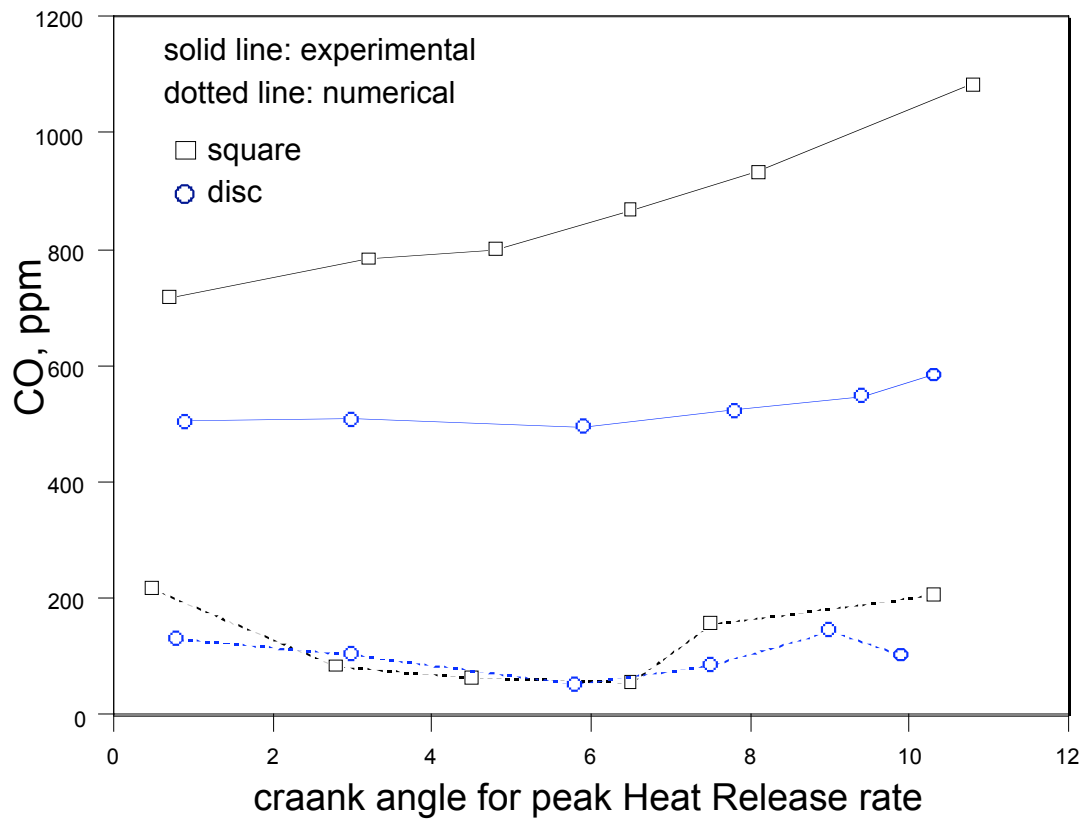
Figure 14. Comparison between experimental and numerical pressure traces for the square geometry. The figure shows experimental pressure traces with solid lines and numerical pressure traces with dotted lines.

Figure 15. Comparison between experimental and numerical heat release rates for the square geometry. The figure shows experimental heat release rates with solid lines and numerical heat release rates with dotted lines.

Figure 16. Ratio between numerical and experimental results for carbon monoxide emissions, hydrocarbon emissions and combustion efficiency, for the disc geometry. A ratio of 1 in the figure indicates perfect agreement between experimental and numerical results.

Figure 17. Comparison between experimental and numerical carbon monoxide emissions as a function of the crank angle for peak heat release, for the square and the disc geometries. The figure shows experimental results with solid lines and numerical results with dotted lines.
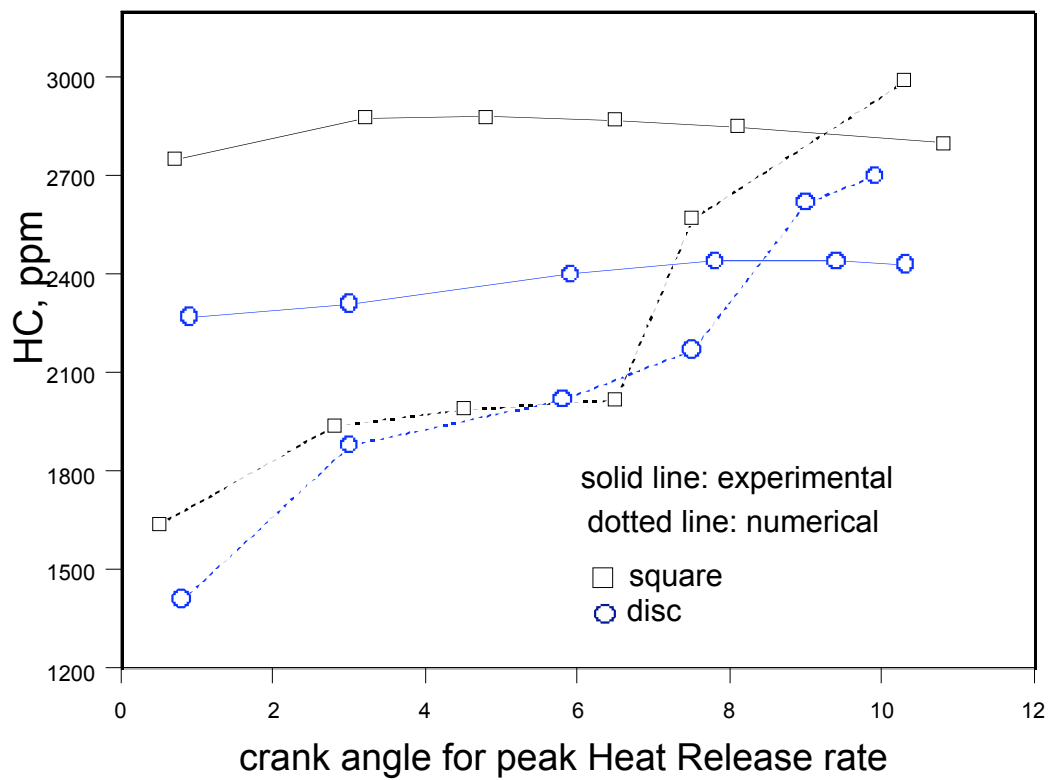
Figure 18. Comparison between experimental and numerical hydrocarbon emissions as a function of the crank angle for peak heat release, for the square and the disc geometries. The figure shows experimental results with solid lines and numerical results with dotted lines.
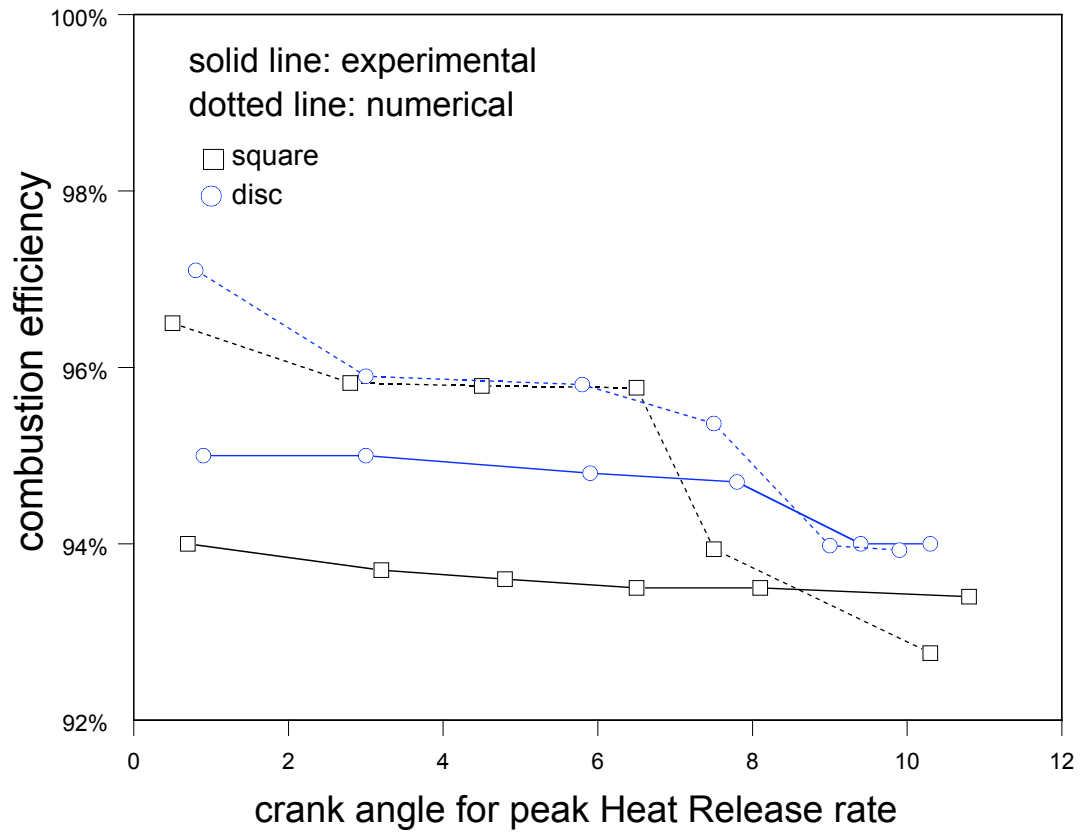
Figure 19. Comparison between experimental and numerical combustion efficiency as a function of the crank angle for peak heat release, for the square and the disc geometries. The figure shows experimental results with solid lines and numerical results with dotted lines.
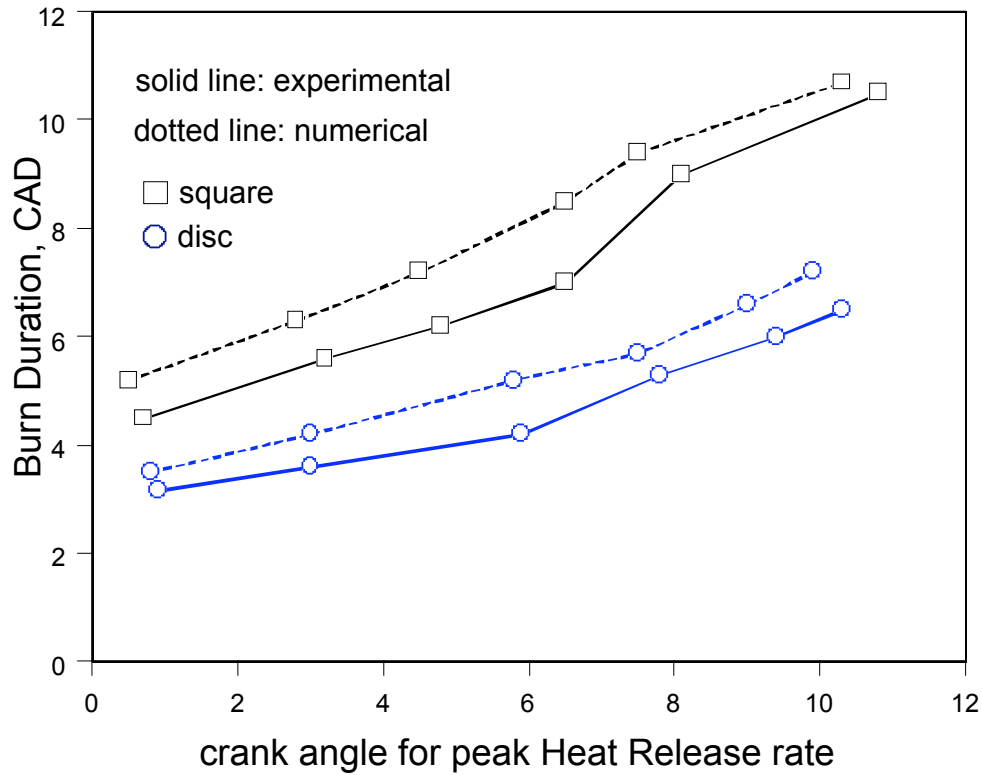
Figure 20. Comparison between experimental and numerical burn duration as a function of the crank angle for peak heat release, for the square and the disc geometries. Burn duration is defined as the crank angle interval between the two points at which the heat release rate is 10% of the peak heat release rate. The figure shows experimental results with solid lines and numerical results with dotted lines.
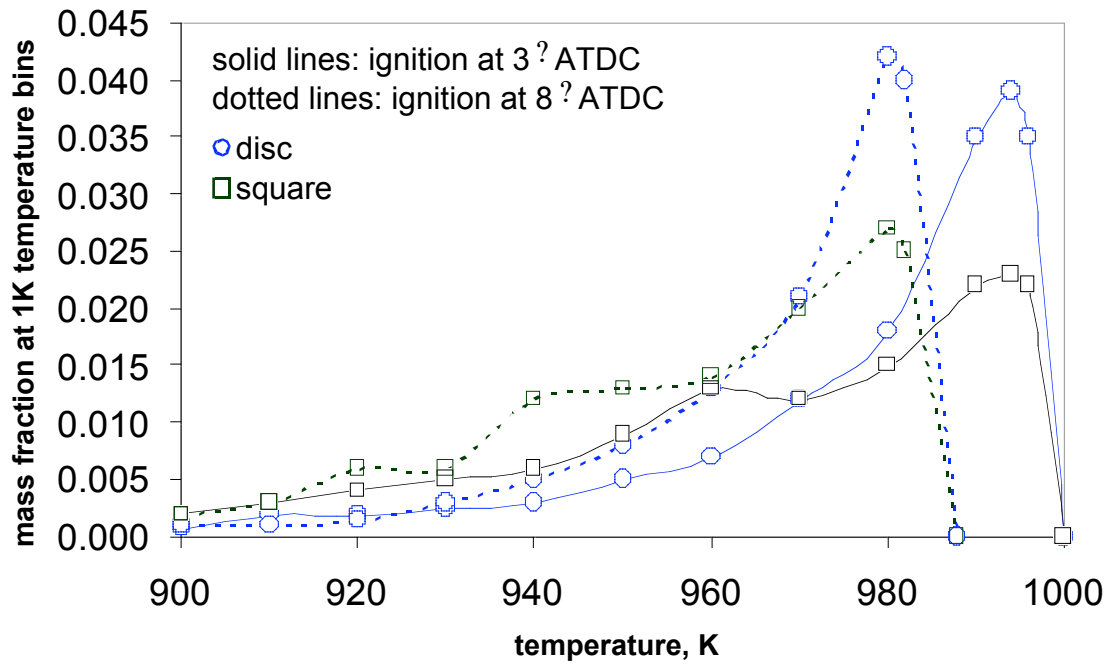
Figure 21. Distribution of mass in temperature space (i.e. what fraction of the total mass exists at any given temperature) at 6 BTDC, for both the square and disc geometries, for two pairs of conditions that have the peak heat release at nearly identical angles. The first pair corresponds to the cases with Tin=443 K for the disc and Tin=431 K for the square geometry. Both of these cases have the peak heat release at ~3 degrees after TDC. Temperature distributions for the first pair are shown with solid lines in the figure. The second pair is Tin=433 K for the disc and Tin=419 K for the square geometry. For this second pair of conditions, peak heat release occurs at ~8 ATDC. Temperature distributions for the second pair are shown with dotted lines in the figure.